Dalton Transactions

Accepted Manuscript

This article can be cited before page numbers have been issued, to do this please use: J. Kobylarczyk, D. Pinkowicz, M. Srebro, J. Hooper and R. Podgajny, *Dalton Trans.*, 2017, DOI: 10.1039/C7DT00293A.

ROYAL SOCIETY OF CHEMISTRY

rsc.li/dalton

View Article Online
DOI: 10.1039/C7DT00293A

Journal Name

ARTICLE

Anion-π recognition between $[M(CN)_6]^{3-}$ complexes and $HAT(CN)_6$: structural matching and electronic charge density modification

Received 00th January 20xx,
Accepted 00th January 20xx

DOI: 10.1039/x0xx00000x

www.rsc.org/

Jedrzej Kobylarczyk, Dawid Pinkowicz, Monika Srebro-Hooper, James Hooper and Robert Podgajny*

Hexacyanidometalates (M = Fe^{III}, Co^{III}) and multisite anion receptor $HAT(CN)_6$ (1,4,5,8,9,11-hexaazatriphenylenehexacarbonitrile) recognize each other in acetonitrile solution and self-assemble into the novel molecular networks $(PPh_4)_3[M(CN)_6][HAT(CN)_6]$ (M = Fe, **1**; Co, **2**) and $(AsPh_4)_3[M(CN)_6][HAT(CN)_6]\cdot 2MeCN\cdot H_2O$ (M = Fe, **3**; Co, **4**). **1**-**4** contains the stacked columns $\{[M(CN)_6]^{3-};[HAT(CN)_6]\}_\infty$ separated by the organic cations. All of the M-C≡N vectors point collectively towards the centroids of pyrazine rings on neighboring $HAT(CN)_6$ molecules, with $N_{cyanide}\cdots centroid_{pyrazine}$ distances that are under 3 Å. The directional character and structural parameters of the new supramolecular synthons correspond with collective triple anion-π interactions between the CN^- ligands of the metal complexes and the π-deficient areas of $HAT(CN)_6$. Physicochemical characterisation (IR spectroscopy, UV-Vis spectroscopy, cyclic voltammetry) and dispersion-corrected DFT studies reveal the dominating charge-transfer (CT) and polarisation characters of the interactions. The electronic density flow occurs from the CN^- ligands of $[M(CN)_6]^{3-}$ to the $HAT(CN)_6$ orbital systems and further, toward the peripheral –CN groups of $HAT(CN)_6$. Solid-state DFT calculations determined the total interaction energy of $HAT(CN)_6$ to be *ca.* -125 kcal·mol^{-1}, which gives *ca.* -15 kcal·mol^{-1} per one $CN^-\cdots HAT(CN)_6$ contact after subtraction of the interaction with organic cations. The UV-Vis electronic absorption measurements prove that the intermolecular interactions persists in solution and suggest a 1:1 composition of the anion-π $\{[M(CN)_6]^{3-};[HAT(CN)_6]\}$ chromophore, with the formation constant $K_{add} = (5.8 \pm 6)\cdot 10^2$ dm^3·mol^{-1} and the molar absorption coefficients $\varepsilon_{add} = 180 \pm 9$ cm^{-1}·dm^3·mol^{-1} at 600 nm, as estimated from concentration-dependent studies.

Introduction

Weaker does not mean *worse*, to paraphrase a popular sentiment, and it is perfectly illustrated by non-covalent interactions,[1] which play a crucial role in the formation and stabilization of molecular platforms as well as in determining their functional character. An important aspect in designing new materials is to exploit such interactions towards recognition between molecular fragments. The formation of specific molecular arrangements occurs through hydrogen bonds, π-π interactions or ion-π adducts assisted by electrostatic interactions, van der Waals interactions and hydrophobic interaction; such interactions are known to reinforce or to work against coordination bonding, and can therefore influence the dimensionality and properties of coordination compounds.[2-10] Coordination complexes can themselves participate in the formation of extended supramolecular systems of various character and function. They serve as building block for supramolecular coordination cages,[11] polymers[12] and nanoscale systems,[13] oligomeric switchable catenane and rotaxane systems,[14, 15] or act as catalytic sites for a variety of organic reactions or biological processes,[16] All of these applications exploit the sophisticated organisation of the complexes' second coordination spheres *via* intramolecular or intermolecular scaffolding.

Faculty of Chemistry, Jagiellonian University in Kraków, Ingardena 3, 30-060 Kraków, Poland.
Electronic Supplementary Information (ESI) available: complete of experimental, analytical, structural (CCDC No. 1515833-1515836), spectroscopic and computational data. See DOI: 10.1039/x0xx00000x

View Article Online
DOI: 10.1039/C7DT00293A

Anion-π systems offer perfect models to study such supramolecular matching and a plethora of elegant examples have been recently reported.[17-20] For the most part, these adducts make use of simple and extended π-acidic systems involving -F,[21] -CN,[22-24] -NO_2[25] (or other) substituted aromatic rings, naphtalenediimides systems,[26-30] polyazines,[18, 31-33] and, recently, some of their N-oxides reported by some of us.[34] Their potential applications include recognition and selective binding of both simple and more extended anions (e.g F^-, Cl^-, Br^-, CN^-, NO_3^-, CO_3^{2-}, ClO_4^-, BF_4^-, PF_6^-, AsF_6^-, SbF_6^-, glutamate, aspartate),[17, 23, 30, 35, 36] controlled formation of macrocyclic oligomeric complexes,[17, 31] catalysis supported by intramolecular covalent scaffolds,[26, 37] tuning of physical response,[38] influencing the magnetic exchange interaction[39, 40] and activity in biological systems.[36, 41] Beyond the systems which include simple anions, little attention has been paid to the binding of the classical Werner anionic complexes. A particular interest could be paid to the polycyanidometalates, as they are important in syntheses of polynuclear cyanido-bridged complexes with interesting magnetic, electron transfer, chiral, spin crossover, or luminescent properties, among others.[5, 42-50] To the best of our knowledge only the groups of Bianchi and López-Garzón performed systematic research on binding parameters for systems {complex;L^1} and {complex;L^1/AC} in solution (complex - octahedral $[M(CN)_6]^{n-}$ (Fe^{II}, Co^{III}) or planar $[Pt(CN)_4]^{2-}$; L1 - pyrimidine derivative substituted with tris(2-aminoethyl)amine, tren; AC – activated carbon).[51] A single very short $_{CN}N\cdots centroid_{pyrimidine}$ contact in the cation assisted intramolecular {$[Co(CN)_6]^{3-}$;pyrimidine} adduct, with the distance of 2.786 Å and angles α_1 = 9.9° and α_2 = 46.2° (*to be discussed below*) was found.[52] Very recently some of us reported the observation of very similar anion-π type contact between $[W(CN)_8]^{3-/4-}$ anion and pyrazine-N,N'-dioxide with the distance $CN\cdots centroid_{pzdo}$ approaching 3 Å.[34] Addressing the obvious need to explore this field further, we are currently interested in the supramolecular interaction and crystal formation between polycyanidometalate complexes and molecules from the prominent HAT (hexaazatriphenylene)-based family.[53] Our first choice herein is the planar molecule $HAT(CN)_6$ (1,4,5,8,9,11-hexaazatriphenylenehexacarbonitrile), which is shown to the right of Fig. 1a.[54] $HAT(CN)_6$ has a specific triangular puzzle-like shaped π-deficient area (colored in blue in Fig.1a), which is granted by three pyrazine rings that are side-condensed to the central benzene ring on the one side, and capped by six –CN substituents around the periphery. This building block offers great potential in constructing systems with a tunable photophysical response in stacked layered composites (e.g. organic light emitting diodes, OLEDs), due to the low-lying LUMO orbitals close to the Fermi level.[38] Recently, it has also been recognized as an efficient multisite triangular anion receptor in THF, CH_3NO_2[23] and MeCN[24] solutions. It has been shown already to create anion-π adducts based on either charge-transfer (CT) systems (Br^-, I^- and SCN^- anions) or electron-transfer (ET) systems (F^-, OH^- and OCN^- anions), in accordance with the increasing strength of Lewis basicity of the anion.[24] $HAT(CN)_6$ and its reduced radical anion form

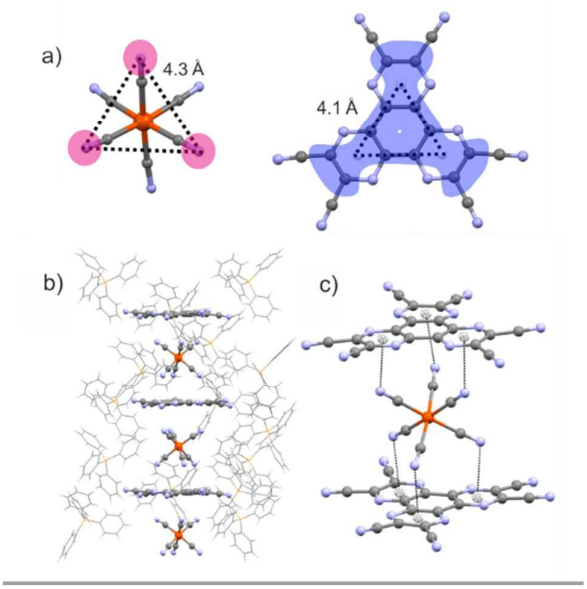

Figure 1. (a) Comparison of average representative distances between nitrogen atoms in cyanides in $[Fe(CN)_6]^{3-}$ or $[Co(CN)_6]^{3-}$ anion (left) and between centroids in $HAT(CN)_6$ (right). The red / blue areas indicate the electron rich / electron deficient regions. (b) Columnar structure of **1**-**4**. (c) Marked anion-π interactions between hexacyanometalate and two neighboring $HAT(CN)_6$.

$HAT(CN)_6^{\bullet-}$ has been very scarcely used in a construction of solid state molecular crystals[55-58] or nanosystems,[22] however, its affinity to the anionic species was documented. The infinite columnar stacked {$anion^-$;$HAT(CN)_6$}$_\infty$ ($anion^-$ = PF_6^-,[56] Br^-,[23] I^- [54]) was observed when the neutral form was incorporated in the crystal. The anion-π synthons were not "saturated", as only a part of π-deficient areas were involved in the anion-π contact in these cases. The classical local binding of PF_6^-, into the {PF_6^-;$HAT(CN)_6$;PF_6^-}$_\infty$ adducts was observed only in the cavity composed of $HAT(CN)_6^{\bullet-}$ and phenyl rings, coordinated/attached to Cu^I centres in {$[Cu^IL]_3[HAT(CN)_6]$} complexes with triple chelating coordination mode Cu^I-(N,N-diimine)$_{HAT}$.[55, 56]

Herein, we report the supramolecular recognition between hexacyanidometalates and $HAT(CN)_6$ towards novel adducts {$[M(CN)_6]^{3-}$;$[HAT(CN)_6]$} in MeCN solution, leading to four new crystalline phases, $(PPh_4)_3[M(CN)_6][HAT(CN)_6]$ (M = Fe, **1**; Co, **2**) and $(AsPh_4)_3[M(CN)_6][HAT(CN)_6]\cdot 2MeCN\cdot H_2O$ (M = Fe, **3**; Co, **4**). **1**-**4** are described using structural, physicochemical and computational (density functional theory (DFT) with both periodic and molecular cluster models) methods. The anion-π synthons are saturated in all four compounds. This, therefore, represents a new approach to observe anion-π interactions between a π-deficient multisite anion receptor $HAT(CN)_6$ and anionic ligands which are pre-organized in a metal complex.

Results and discussion

Synthesis and crystal structures

View Article Online
DOI: 10.1039/C7DT00293A

Combining $A_3[M(CN)_6]$ (A = PPh_4^+, $AsPh_4^+$; M = Fe^{III}, Co^{III}) salts with $HAT(CN)_6$ we present a new example of *pre-programmed* supramolecular self-assembly. These building blocks match structurally and electronically: both the centroids of $HAT(CN)_6$, with well determined π-deficient regions, and the *fac*-oriented anionic cyanides of $M(CN)_6$ form equilateral triangles with very similar edge lengths (Fig. 1a). The needle shape crystals of 1-4 were obtained by a slow diffusion of diethyl ether into a MeCN solution of the reactants. **1** and **2** crystallize in the trigonal system, space group *R*3*c*, while **3** and **4** crystallize in the monoclinic system, space group *Cc*. The detailed crystallographic data and metric parameters are presented in Figures S1-S6 and Tables S1-S4 (ESI†). The uniformity **1**-**4** was confirmed by PXRD measurements (Figures S7-S10, ESI†). The stability of **1** and **2** up to 100 °C was determined by TGA measurements and PXRD measurements (Figures S7-S12, ESI†). All compounds reveal a columnar structure with straight $\{HAT(CN)_6;[M(CN)_6]^{3-}\}_\infty$ supramolecular chains that are surrounded and separated by the bulky organic cations (Fig. 1b), and, in the case of **3** and **4**, additionally supported by MeCN and H_2O molecules. The novel feature in **1**-**4** is definitely the orientation of N atoms of all CN^- ligands towards the centroids of pyrazine rings in $HAT(CN)_6$, forming an unprecedented sandwich arrangement of triple M-C-N···$centroid_{pyrazine}$ supramolecular linkages for each complex (Fig. 1c). Each side of $HAT(CN)_6$ is thus accepting all three N atoms of the three *fac* oriented cyanides, with N···centroid distances of 2.952 and 2.990 Å (**1**), 2.945 and 2.989 Å (**2**), 2.90-3.16 Å (**3**) and 2.91-3.20 Å (**4**). Such mutual orientation is a natural consequence of the highlighted molecular matching. A similar, but less saturated, stacking of $HAT(CN)_6$ was observed recently by Dunbar et al. in $\{([n\text{-}Bu_4N][Br])_3[HAT(CN)_6]\}\cdot 3C_6H_6$ compound, where Br^- anions were positioned above and below the saturated C-C fragments of $HAT(CN)_6$ with a non-complete occupation.[23] The $[M(CN)_6]^{3-}$ units have only slightly distorted octahedral geometry (Table S5, ESI†). The Fe-C and Co-C distances are 1.95-1.97 and 1.91-1.92 Å, respectively, which are notably longer (by 0.02-0.04 and 0.01-0.02 Å) than related reference $[M(CN)_6]^{3-}$-based compounds. At the same time, the M-C-N angles keep their usual linearity of 175-180°. The observed subtle shift of the CN^- ligands from the complex towards the $HAT(CN)_6$ centroids is interpreted as evidence of an anion-π interaction. The oxidation state of Fe^{III} in **1** was confirmed by magnetic moment measurements and ^{57}Fe Moessbauer spectroscopy (Figure S13, ESI†).

For a complete and exact description of the Fe-C-N···$centroid_{pyrazine}$ synthons we examined angles of incidence at each CN^-···$HAT(CN)_6$ contact, α_1 and α_2, with respect to *d*, the distance between CN^- vector and $HAT(CN)_6$ centroid (Fig. 2a), according to the protocol proposed recently by Bianchi et al.[52] (see also ESI†). The full set of results for compounds **1**-**4** is presented in Figs. 2b,c and in Table S6 (ESI†). Compared to the structural data obtained from a CSD search for $[M(CN)_6]$ based compounds (black points in Figs. 2b,c), the geometrical parameters of the contacts in 1-4 with $\alpha_1 < 15°$ and $\alpha_2 < 65°$, allow them to be classified as a group of compounds with significant anion-π interactions between a multisite anion receptor ($HAT(CN)_6$) and the three CN^- anions that are pre-organized within each adjacent $[M(CN)_6]^{3-}$ complex. The spread of data points in Fig. 2 illustrates how the crystal structure affects the anion-π interactions; the *d*, α_1, and α_2 parameters are only subtly different in **1** and **2**, but much more spread out in compounds **3** and **4** (ESI†). Their variance relates to the degree to which $HAT(CN)_6$ bends in the crystal lattice; this is a small effect in **1** and **2** but there is a severe bending of one –CN group when it is crystallized with solvent H_2O molecules in **3** and **4**.

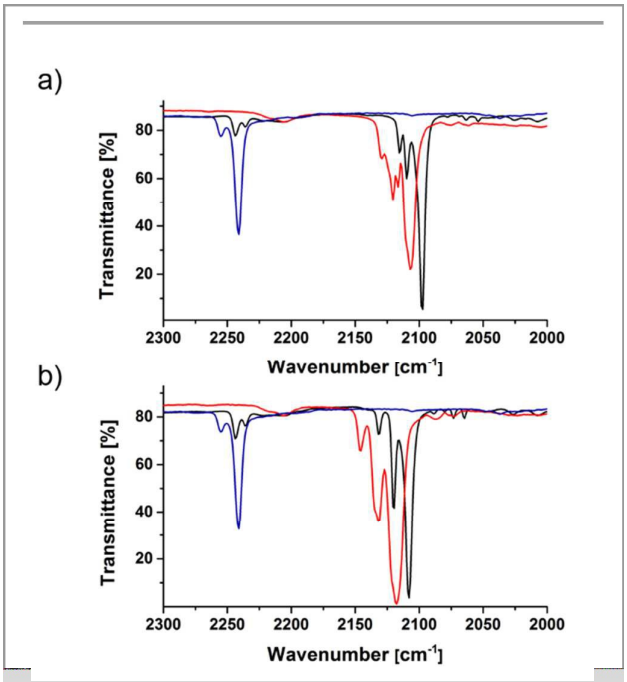

Figure 3. IR spectra of **1** (a) and **2** (b) (black line), the reference starting complexes $(PPh_4)_3[Fe(CN)_6]\cdot 6H_2O$ (a) or $(PPh_4)_3[Co(CN)_6]\cdot 7H_2O$ (b) (red lines), and $HAT(CN)_6$ (blue lines) in the ν(C≡N) range.

View Article Online
DOI: 10.1039/C7DT00293A

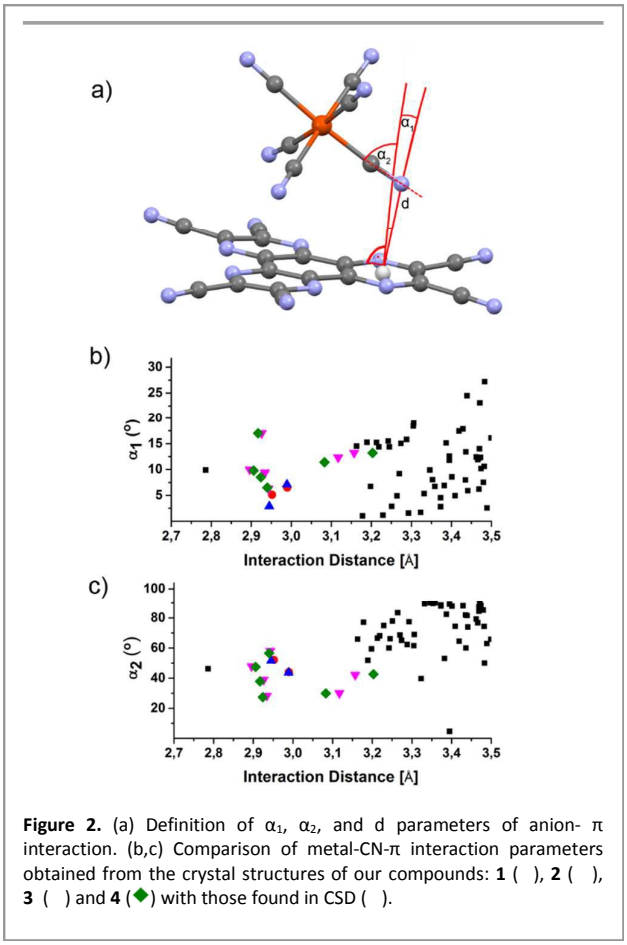

Figure 2. (a) Definition of α_1, α_2, and d parameters of anion- π interaction. (b,c) Comparison of metal-CN-π interaction parameters obtained from the crystal structures of our compounds: **1** ( ), **2** ( ), **3** ( ) and **4** (◆) with those found in CSD ( ).

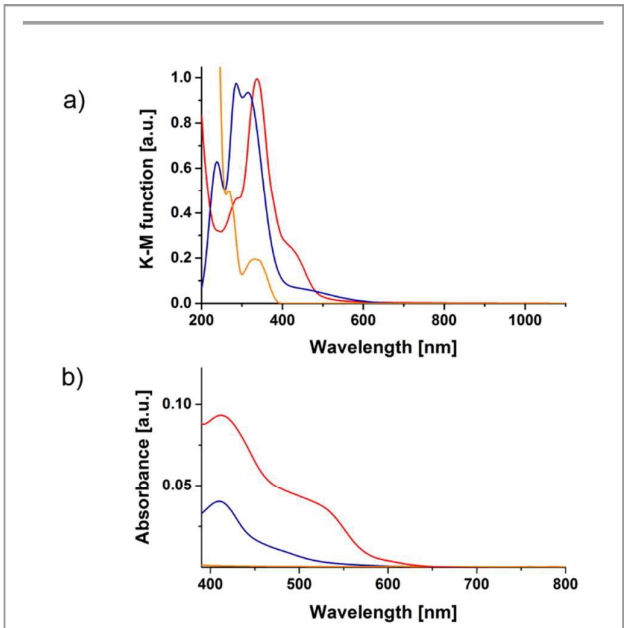

Figure 5. Electronic UV-Vis spectra of **2** and its precursors in solid state as K-M functions (a), and in MeCN solution (b). Concentration of precursors was set to 0.65 mmol·dm^3. Colours: $(PPh_4)_3[Co(CN)_6]\cdot 7H_2O$ (yellow), $HAT(CN)_6$ (blue), and **2** (red)

IR spectroscopy

The IR spectra of **1** and **2** in *ν*(C≡N) region, 2250-2200 cm^{-1} for –CN groups and 2200-2000 cm^{-1} of CN^- ligands, show a general weakening of the vibrations compared to their precursors (Fig. 3, Figures S14-S19, ESI†). In the case of $HAT(CN)_6$ vibrations, two peaks appear at 2244 (w) and 2235 (w) cm^{-1} in place of higher energy 2255 cm^{-1} (w) and 2241 cm^{-1} (s) ones. This may be assigned to the decrease of the overall bond order of C≡N group due to an increase in the electronic density on delocalised π*-systems of $HAT(CN)_6$ in the adducts (see also below), in the perfect agreement with the vibrational data reported for reduced $HAT(CN)_6^-$ compounds.[56, 58] In the case of $[M(CN)_6]^{3-}$ complexes the whole spectral patterns are systematically shifted of *ca.* 10-15 cm^{-1}, which is interpreted in terms of weaker binding of CN^- by M inferred from the structural data. This supports strongly the existence of anion-π interaction along the observed structural synthons. The individual absorption wavenumbers, lower for Fe^{III} than for Co^{III}, are in agreement with the binding strength tendency expected for t_{2g}^5 and t_{2g}^6 configurations, respectively.

UV-Vis spectroscopy

While the color of starting organic salts is yellow (Fe) or smoked white (Co), the crystals of **1** and **3** (Fe) are dark green and those of **2** and **4** (Co) are yellow, which suggest the significant spectral modifications in UV-VIS range (Figs. 4 and 5, Figs. S20-S21, ESI†). Similar colors were found for the MeCN solutions of **1** and **3**, and **2** and **4**, respectively. The representative UV-VIS electronic absorption spectra are presented in Fig. 4 and Fig. 5 for **1** and **2**, respectively; the panels in (a) show the Kubelka-Munk (K-M) functions for the solid state, while in the panels in (b) show the corresponding spectra in MeCN solutions. The strong UV-Vis bands in the solid state absorption of **1** in the 200 – 470 nm range (λ_{max} of 240, 330 and 415 nm) can be assigned to the sum of the intraligand (IL) transitions within $HAT\text{-}CN_6$[24, 58] and ligand-to-metal charge-transfer (LMCT) transitions from CN^- to Fe^{3+},[59] with slightly modified energy due to the nature of intermolecular interactions in the solid state. In the case of **2**, a strong absorption of $HAT(CN)_6$ dominates below 400 nm, covering the ligand-field (LF) bands for $[Co(CN)_6]^{3-}$.[59] The new broad visible absorption bands are easily seen for **1** in the range of 500-800 nm, appearing at λ_{max} 600 nm. The similar additional intensity can be also observed in the case of **2**, but the corresponding bands are strongly blue-shifted comparing to **1**, i.e. to 400-650 nm with λ_{max} of *ca.* 440 nm(sh) (overlapping with the absorption of $HAT(CN)_6$).

The appearance of such additional broad absorption bands in the visible spectral region (up to 600-700 nm) was found to be also characteristic for relatively *stable* adducts composed of octacyanidotungstates(V) and cationic species. It occurs in specific circumstances, e.g. when nitrogen atoms of C-coordinated CN^- ligands are in a close frontal electrostatic contact with *s* metal cations (Li^+-Cs^+). This is generally seen for such solid-state salts, as well as for Na^I- or K^I-Mn^{II}_2(pzdo)-$[W^V(CN)_8]^{3-}$ adducts in aqueous solution.[34] Contrary to that, none or very poor visible absorption is

DOI: 10.1039/C7DT00293A

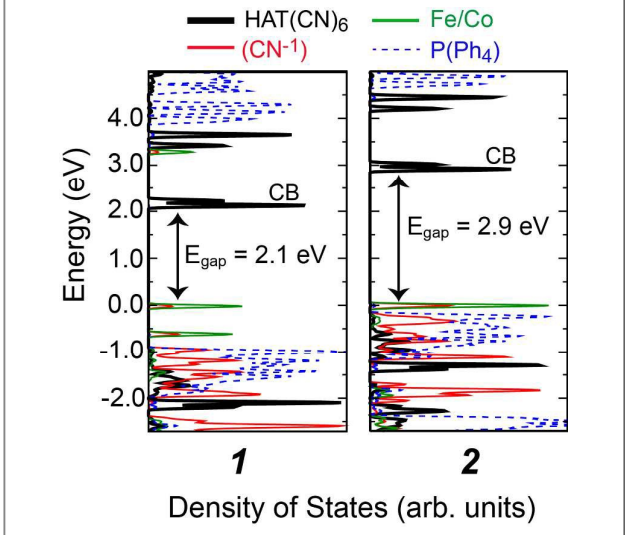

Figure 6. The computed (DFT/HSE06[62]) electronic band energies of **1** (right) and **2** (left). The Fermi energy is set to zero in each plot. The lines are colored according to the projection of the electronic band structure onto the atoms of the molecular building blocks. The location of the conduction band (CB) is shown in each plot. See also ESI†.

(yellow), $HAT(CN)_6$ (blue), and **1** (red)

seen for solutions of $[W(CN)_8]^{3-}$ salts or its organic salts, e.g. $TBA_3[W(CN)_8]$ in solid state. A distinguishable visible absorption may also occur due to the donor-acceptor interaction involving polycyanidometalates, which was shown for $[Pt^{II}L_n]^{2+}$-$[W^{V}(CN)_8]^{3-}$ [L_n = $(NH_3)_4$, $(en)_2$] systems, as well as for the range of cyanidometalate-based systems.[60, 61]

Accordingly, we tentatively link the new absorption bands observed for **1** and **2** to the anion-π CT interaction between the CN^- ligands in the metal complexes and the π-deficient electron system of the $HAT(CN)_6$ molecule. This appears to be qualitatively supported by the calculated electronic structure of **1** and **2**. The computed (DFT,[62] periodic conditions) electronic band energies of both systems are shown in Fig. 6; see the ESI† for computational details and additional calculated results. The peaks in Fig. 6 are colored according to which fragments contribute to each energy level, and the energy levels are scaled such the highest occupied electronic state is assigned to 0 eV. It is clearly seen that the lowest unoccupied energy levels, i.e. the conduction bands (CB's), correspond with $HAT(CN)_6$ electronic states, and that the highest occupied energy levels correspond with $[M(CN)_6]^{3-}$ states. This is consistent with the $M/CN^- \rightarrow HAT(CN)_6$ CT assignment of the new long-wavelength adsorption bands. Furthermore, the presence of unpaired spin density in **1** results in a smaller band gap; 2.1 eV for **1** (with a spin-doublet d^5 electronic configuration of Fe) vs. 2.9 eV for **2** (with a closed-shell d^6 configuration of Co). This nicely correlates with the experimentally observed bathochromic shift of low-energy adsorption bands for **1** as compared to **2**.

The colors and spectra of the MeCN solutions of **1**-**4**, with similar additional broad absorption bands at λ_{max} = 540, 600 nm (for **1**) and λ_{max} = 500, 590 nm (for **2**) indicate preservation of anion-π contacts

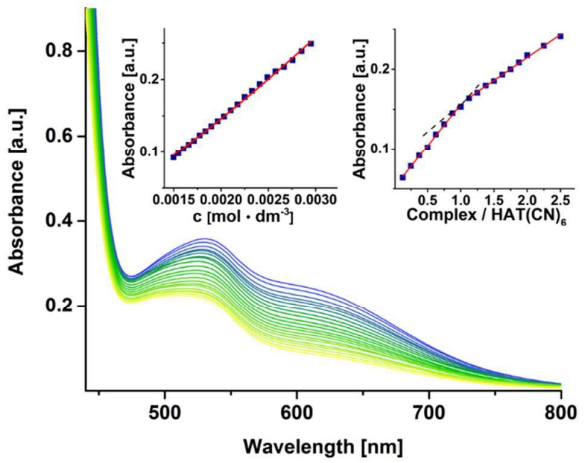

Figure 7. Evolution of visible electronic absorption spectrum of **1** dissolved in MeCN upon decrease in concentration of adduct within *c* range of $1.5\text{-}3.0\cdot10^{-3}$ mol·dm^3 Inset: the fitted $A_\lambda(c_1)$ dependence (left) and the Joe-Jones plot (right) for λ = 600 nm.

after dissolution. The absorption is of rather moderate intensity and it strongly resembles that presented by Ballester *et al.* for the CT contact pairs {anion$^-$;$[HAT(CN)_6]$} engaging weak nucleophilic anions as Br^-, I^- or SCN^-.[17,23,24] This indicates a relatively weak electrophilic character of CN^-, while C-coordinated to the metal ion, and supports anion-π CT assignment of the solid-state adducts. As reference studies, we performed the UV-Vis titration of $HAT(CN)_6$ with free CN^- anion provided by TBA^+CN^- salt or with $[Fe(CN)_6]^{3-}$ and $[Co(CN)_6]^{3-}$. In the former case, the sequential appearance and disappearance of absorption peaks at λ_{max} = 761, 690 and 630 nm characteristic for the reduced $HAT(CN)_6^{\bullet-}$ was observed (see Fig. S22, ESI†)[24, 58] suggesting the redox pathway from the CT $\{CN^-;HAT(CN)_6\}$ adduct through the radical anion $HAT(CN)_6^{\bullet-}$ towards the dianion $HAT(CN)_6^{2-}$ and/or possible unrecognized products of its decomposition.[24] Such electron-transfer (ET) behaviour was observed when the strong electrophiles such as HO^-, F^-, or OCN^- were used for a titration. With $[Fe(CN)_6]^{3-}$ and $[Co(CN)_6]^{3-}$ used as a titrant no spectral signatures for $HAT(CN)_6^{\bullet-}$ were observed in the UV-Vis absorption which may be due to weakening of Lewis basicity and suppression of kinetic movements of coordinated CN^-, in comparison to the free CN^-.

Interestingly, the $HAT(CN)_6^{\bullet-}$ electronic absorption characteristics can be observed for the MeCN solutions of **2**, as well as for the solid-state samples of **2,** exposed to UV-Vis light irradiation. It is expected that the extent of redox reaction should be rather dependent on the light intensity and degree of diffusion. Preliminary results indicate that the effect is stronger in the case of **2**, which can be tentatively assigned to the facile release of cyanide from $[Co(CN)_6]^{3-}$ complexes under the 365 nm irradiation.[63] At the same conditions, no or very little ET was exhibited by the solutions of **1**, probably due to the different character of its absorption spectra compared to **2**. As this are the very preliminary results, the above photophysical phenomena could be studied in details in future work.

View Article Online
DOI: 10.1039/C7DT00293A

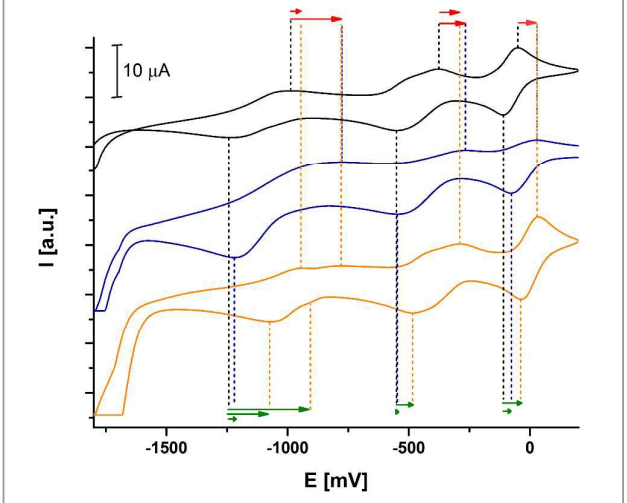

Figure 8. Cyclic voltammograms for $HAT(CN)_6$ (black), compound **1** (blue), compound **2** (orange), versus Ag/AgCl in MeCN. Concentrations: $(Bu_4N)PF_6$, 0.1 M; **1** and **2**, 0.002 M. The arrows show the shift of the potential waves.

To estimate a character and a degree of association between $HAT(CN)_6$ and $[M(CN)_6]^{3-}$, dependence of absorbance A_λ on the molar ratio complex:$HAT(CN)_6$, *n*:1, (so called Joe-Jones method) and on the concentration of adduct *c*, at the selected wavelengths λ in the novel absorption range was carefully studied (Fig. 7). We have selected the $\{Fe(CN)_6]^{3-}$;$HAT(CN)_6\}$ adduct as its diagnostic absorption above 550 nm did not interfere with the absorption of the precursors. The $A_{600\ nm}(n)$ curve suggest the formation of 1:1 adduct with a moderate formation constant, as can be deduced from the slopes of $A_{600\ nm}(n)$ on both sides of the critical point. Indeed, the fitting of $A_{600\ nm}(c)$ curve for the solution of **1** with the equation derived for 1:1 adduct gave the reasonable set of values of the formation constant K_{add} = (5.8 ± 6)·10^2 $dm^3 \cdot mol^{-1}$ and molar absorption coefficients ε_{add} = 180 ± 9 $cm^{-1} \cdot dm^3 \cdot mol^{-1}$ (see eq. 1, ε_s – the molar absorption coefficient of the substrates, c_{tot} – total concentration of substrates).[60]

The coexistence of other adducts cannot be however excluded and thus, the presented data should be treated with caution as the first approximation of adduct formation in the solution.[64]

Cyclic voltammetry

The cyclic voltammograms of **1** and **2** show generally three redox waves assignable to the $HAT(CN)_6$ (Fig. 8, Table S8 ESI†).[57,58] For **2** the notable shift of *ca.* 100 mV towards higher potential values is observed, while the shape of the signal is reasonably preserved. In the case of **1** the intensity of the oxidizing waves $HAT(CN)_6^{2-}/HAT(CN)_6^-$ and $HAT(CN)_6^-/HAT(CN)_6$ is significantly reduced, which may be due to the interference with redox pair $[Fe(CN)_6]^{3-/4-}$. The direct observation of the latter redox pair is difficult due to its relatively weak signal at the conditions applied. A general increase of redox potentials of $HAT(CN)_6$ indicates the increase of electronic density on its aromatic systems, in line with the claimed CT transfer character of our anion-π synthons.

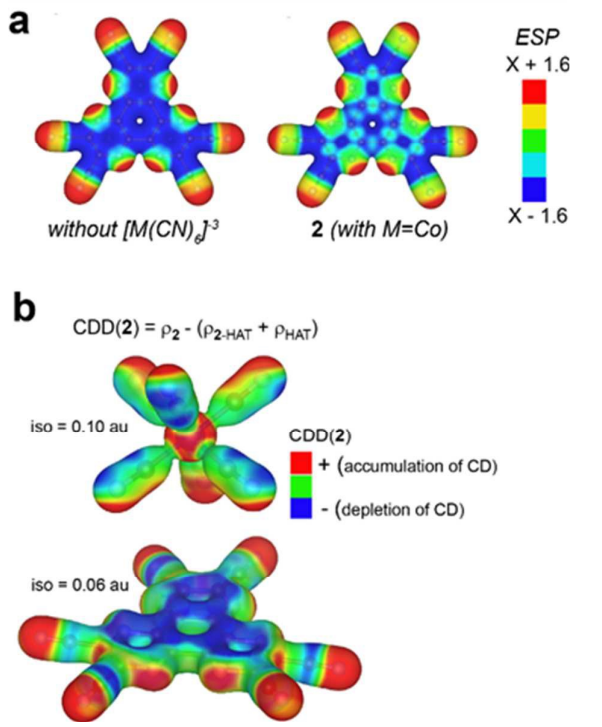

Figure 9. (a) The computed electrostatic potential (ESP) around $HAT(CN)_6$ in two chemical environments: in the $HAT(CN)_6$ / PPh_4^+ sublattice of **2** when the P atoms are substituted with Si atoms (left), and in **2** (right). The ESP is coloring an isosurface of the total electron density from a single $HAT(CN)_6$ molecule (isovalue of = 0.02 au); X is the middle of the range of ESP values which are sampled on the isosurface. (b) The charge density difference (CDD) surrounding a $HAT(CN)_6$ molecule (bottom) and a $[M(CN)_6]^{3-}$ molecule (top) in **2**.The CDD is coloring an isosurface of the total electron density from a single $HAT(CN)_6$ or $[M(CN)_6]^{3-}$ molecule.

Theoretical study of the anion-π interactions

$$A_{600} = \varepsilon_s c_{tot} + \frac{(\varepsilon_{add} - \varepsilon_s)\left[1 + 2K_{add}c_{tot} - (1 + 4K_{add}c_{tot})^{\frac{1}{2}}\right]}{2K_{add}} \quad (eq.\,1)$$

To gain deeper insight into the electronic structure of these unprecedented complexes **1**-**4**, dispersion-corrected (DFT-D3)[65] calculations have been performed for both periodic[66, 67] and molecular cluster models[68-70] (see ESI†). The calculated (PBE-D3, periodic conditions) interaction energies ΔE_{int} of $HAT(CN)_6$ with the surrounding chemical environment, i.e. with the adjacent $[M(CN)_6]^{3-}$ complexes and the surrounding cations and/or solvent molecules, were found to be -124, -126, and -126 $kcal \cdot mol^{-1}$ for compound **1**, **2**, and **4** respectively. The estimated strength of the interaction between $HAT(CN)_6$ and the nearby $[M(CN)_6]^{3-}$ metal complexes is -78 $kcal \cdot mol^{-1}$ in **1** and -81 $kcal \cdot mol^{-1}$ in **2** and **4**. This amounts to the anion-$HAT(CN)_6$ interactions making up most of the total interaction energy (over 60%) and, furthermore, suggests that the net

View Article Online
DOI: 10.1039/C7DT00293A

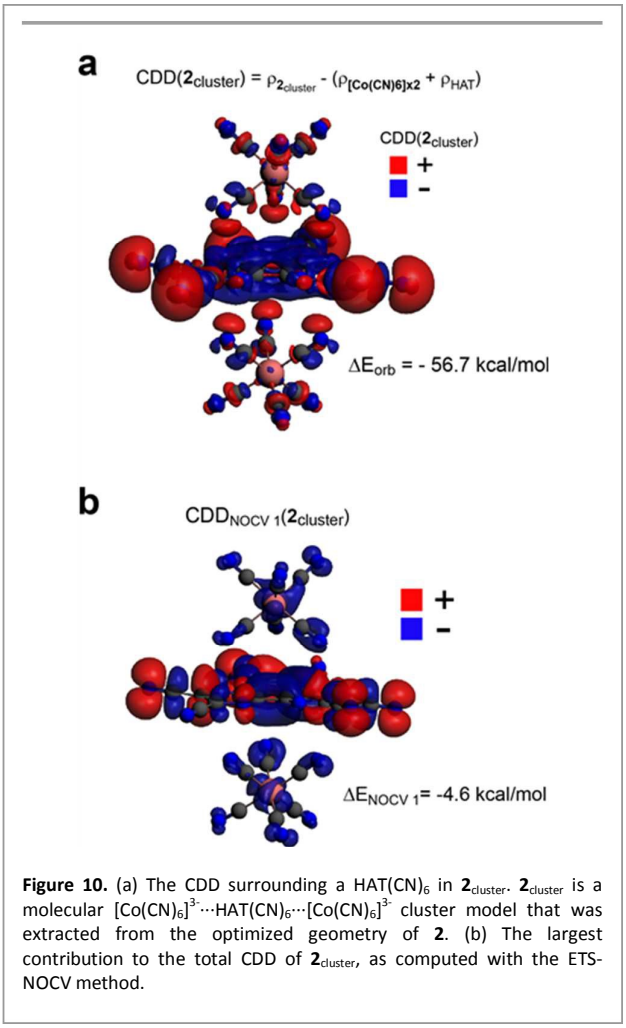

Figure 10. (a) The CDD surrounding a $HAT(CN)_6$ in $\mathbf{2}_{cluster}$. $\mathbf{2}_{cluster}$ is a molecular $[Co(CN)_6]^{3-}\cdots HAT(CN)_6\cdots[Co(CN)_6]^{3-}$ cluster model that was extracted from the optimized geometry of **2**. (b) The largest contribution to the total CDD of $\mathbf{2}_{cluster}$, as computed with the ETS-NOCV method.

interaction strength induced by each $M\text{-}CN^{-}\cdots HAT(CN)_6$ contact is moderate, -15 kcal·mol^{-1} per contact (ESI†). The similar interaction energies suggest that the metal complexes, and the accompanying cations, have a similar overall influence on $HAT(CN)_6$ and that the $CN^{-}\cdots HAT(CN)_6$ anion-π interactions are crucial and consistent in guiding the formation of each structure. In Fig. 9, the computed profiles of the electrostatic potential (ESP) around $HAT(CN)_6$ are shown in two periodic environments, the rightmost of which corresponds to $HAT(CN)_6$ embedded in **2**. Both ESP profiles show the expected electron-deficient regions (coded as dark blue) over the center of $HAT(CN)_6$ and the electron-rich regions (red) around its periphery. The metal complex in **2** causes slight, but tangible, increases in the ESP above the center of $HAT(CN)_6$. This may indicate the charge transfer (CT) donation from the electron-rich $[M(CN)_6]^{3-}$ complex to $HAT(CN)_6$. Bader charge analysis indicates that $HAT(CN)_6$ accumulates only a slight negative charge in the crystal structures, computed at -0.05 *e* for both **1** and **2**, -0.07 *e* for **4**. The redistribution of electronic density, i.e. the charge deformation density (CDD), around $HAT(CN)_6$ and $M(CN)_6$ when $HAT(CN)_6$ is inserted into **2** is shown in Fig. 9. The most prominent feature of the CDD is an increase in electron density (coded as red) around the CN groups in $HAT(CN)_6$ and a decrease in electron density (blue) over its center, presumably enabling the $HAT(CN)_6$ to form stronger C-H···N type hydrogen bonding with the cations and to enhance the anion-π interactions.

The features of the CDD around $HAT(CN)_6$ and $[M(CN)_6]^{3-}$ in **2** are captured quite well with a simple molecular cluster, a $[Co(CN)_6]^{3-}\cdots HAT(CN)_6\cdots[Co(CN)_6]^{3-}$ sandwich, that was extracted directly from the optimized coordinates of **2** (Fig. 10a). With this molecular cluster ($\mathbf{2}_{cluster}$), we used the ETS-NOCV method[71] to decompose the CDD into chemically-intuitive orbital-based contributions from the fragments' molecular orbitals. This allows us to comment to a degree on the nature of the interaction between $HAT(CN)_6$ and adjacent $[Co(CN)_6]^{3-}$. In Fig. 10b, the largest NOCV contribution to the total CDD is shown; it corresponds to a visible CT donation from $[Co(CN)_6]^{3-}$ to $HAT(CN)_6$ which decreases the charge density on the metal complex, and a strong charge redistribution (polarization, intrafragment CT) within $HAT(CN)_6$ which increases the charge density on its CN groups. The contribution of the first six NOCV's are similar in this regard and, together, contribute -25 kcal·mol^{-1} to the total orbital energy contribution that comes about from the CDD, which is ΔE_{orb} = -56.7 kcal·mol^{-1}. This is consistent with the main response of $HAT(CN)_6$ in **2** being a redistribution of the electron density in $HAT(CN)_6$ accompanied by a slight decrease in charge over the $[M(CN)_6]^{3-}$ complex, as was suggested by the computed charges.

Experimental

Materials

The organic salts of $[M(CN)_6]^{3-}$ complexes were prepared through a metathesis reaction of the potassium salts with the chlorides of organic cations. $HAT(CN)_6$ was synthesised according to the literature protocol.[72] Purity of obtained complexes was checked by elemental analysis, IR spectra and NMR spectra. $AsPh_4Cl$, PPh_4Br, $K_3[Fe(CN)_6]\cdot 3H_2O$, $K_3[Co(CN)_6]\cdot 3H_2O$, and solvents were purchased from commercial sources (Sigma-Aldrich, Alfa Aesar etc.) and used without further purification.

General synthetic procedure for 1-4

The synthesis and all manipulation with **1**-**4** and their solutions were performed in darkness, due to possible photoreactivity (*see* the **UV-Vis spectroscopy** section). Acetonitrile solutions of the organic salts hydrate of a general formula $A_3[M(CN)_6]\cdot xH_2O$ (A = PPh_4^+, $AsPh_4^+$; M = Fe, Co; x = 5-7) were mixed with the acetonitrile solution of $HAT(CN)_6$, to give a dark-green (**1**, **3**) or yellow (**2**, **4**) solution immediately. The solution was stirred for 30 min. The green (**1**, **3**) or yellow (**2**, **4**) crystals suitable for crystallographic measurements were obtained by diffusion of diethyl ether vapour into this mixture. After 1 day, they were filtrated and washed with small amount of cold acetonitrile (4ml, -10°C) and dried in air. **1**-**4** are soluble in acetonitrile. **1** and **2** are air stable, while **3** and **4** cracks after solvent removal to produce **3des** and **4des**, thus the crystallographic measurement were performed for samples moisturized by solvent or in the Apiezon grease. The formulas were determined using SC XRD and elemental analysis. The detailed information is included in ESI†.

View Article Online
DOI: 10.1039/C7DT00293A

Physical techniques

Infrared spectra (IR) were measured tiny crystalline object or powder samples in the 3500 – 675cm^{-1} range using Nicolet iN10 MX FTIR microscope, in transmission mode. NMR spectrum was measured on Bruker Avance III 300 MHz. Elemental analyses were performed on Elementar Vario Micro Cube CHNS analyzer. UV-VIS-NIR measurements in solution and solid state were carried out with PerkinElmer Lambda 35 spectrophotometer. Magnetic measurements were performed on Quantum Design MPMS-3 Evercool magnetometer. Cyclic voltammograms were recorded using a standard 3 electrode systems with Pt 1.6 mm as a working electrode, Pt wire 0,5 mm as an ancillary electrode and Ag/AgCl as a reference electrode, with measured value of ferrocene/ferrocinium redox potential of +0.42V.[58] The supporting electrolyte was tetrabutylammonium hexaflurophosphate ($TBAPF_6$). Thermogravimetric studies were carried out using Mettler Toledo TGA1. P-XRD patterns were measured on a PANalytical X'Pert PRO MPD diffractometer with a capillary spinning add-on using Cu-K_α radiation source. The geometry of coordination polyhedrons were calculated in SHAPE v2.1 program (ESI†).[73]

Crystal structure solution and refinement

All diffraction data were collected at 120 K using Bruker D8 Quest Eco Photon 50 CMOS diffractometer equipped with Mo-K_α radiation source, graphite monochromator and Kryoflex II low temperature device. Data reduction, cell refinements and absorption correction were performed employing Apex suite programs, including SAINT and SABADS. Intensities of reflections were corrected using the multi-scan method. The structure was solved by direct methods and refined anisotropically with weighted full-matrix least squares on F^2. All solved and refined operations were carried out using shelXT and shelXL programs with Olex 2 graphic interface.[74] The selected crystal data and structure refinement are shown in Tables S1 and S2 (ESI†)

Conclusions

In conclusion, we have described, with both experiment and computation, the first example of an anion-π charge transfer (CT) systems between anionic complexes and a multisite anion receptor in solid state and in solution. The features of structural contacts with $N_{cyanide}\cdots centroid_{pyrazine}$ distances < 3 Å and preferential mutual orientation allow to establish the group family of the anion-π systems and fill the existing gap between the only one known $[Co(CN)_6]^{3-}\cdots$(tris(2-aminoethyl)amine-substituted pyrimidine) system and non-anion-π contacts found in other cyanometalate-based systems. The electronic density transfer pathway from cyanide ligands of $[M(CN)_6]^{3-}$ complexes towards the π-deficient regions of $HAT(CN)_6$ and further towards its –CN groups was assigned using DFT methods, in qualitative agreement with the results of spectroscopic data. The calculations of the supramolecular interaction energy in the crystal gave the reasonable values of local interactions between C-coordinated CN^- ligands and of the π-acidic $HAT(CN)_6$, *ca.* 15 kcal·mol^{-1} per one $CN^-\cdots HAT(CN)_6$ contact. The formation of 1:1 $\{Fe(CN)_6]^{3-};HAT(CN)_6\}$ anion-π adduct was suggested with formation constant K_{add} = (5.8 ± 6)·10^2 dm^3·mol^{-1} and molar absorption coefficients ε_{add} = 180 ± 9 cm^{-1}·dm^3·mol^{-1} at 600 nm, which settle in the range observed for other anion-π CT adduct. Our results represent an elegant and successful prediction of structural and electronic matching based on the features of the building blocks. Our study is an important step towards recognition and controlled binding of $[M(CN)_x]^{n-}$ in solution. While further research on more efficient anionic complex binding systems are now underway in our group, we suggest that such anion-π synthons could influence the synthesis of cyanide-bridged functional materials.

Acknowledgements

We gratefully acknowledge the financial support of the National Science Centre (Poland) research project number UMO-2014/15/B/ST5/02098. We thank dr Marcin Kozieł and Bernard Czarnecki (Faculty of Chemistry, Jagiellonian Universty) for help in PXRD and magnetic measurements. We are grateful to prof. Jan J. Stanek (Faculty of Physics, Astronomy and Applied Computer Science of the Jagiellonian University) for ^{57}Fe Mössbauer measurements. M. S.-H. and J.H. acknowledge 'Outstanding Young Scientist' scholarships from the Ministry of Science and Higher Education in Poland. Measurements were carried out with the equipment purchased thanks to the financial support of the European Regional Development Fund in the framework of the Polish Innovation Economy Operational Program (contract no. POIG.02.01.00-12-023/08). Magnetic measurements were performed using the equipment purchased from the Large Research Infrastructure Fund of the Polish Ministry of Science and Higher Education (decision no. 6350/IA/158/2013.1) .

Notes and references

1. K. Liu, Y. Kang, Z. Wang and X. Zhang, *Adv. Mater.*, 2013, **25**, 5530-5548.
2. G. A. Timco, T. B. Faust, F. Tuna and R. E. P. Winpenny, *Chem. Soc. Rev.*, 2011, **40**, 3067-3075.
3. K. Harris, D. Fujita and M. Fujita, *Chem. Commun.*, 2013, **49**, 6703-6712.
4. A. Alessandro, G. Damiano, M. Matteo and D. C. Luisa, *Chem. Let.*, 2015, **44**, 1152-1169.
5. B. Nowicka, O. Stefańczyk, D. Pinkowicz, S. Chorazy, R. Podgajny, and B. Sieklucka, *Coord. Chem. Rev.*, 2012, **256**, 1946-1971.
6. M. Castellano, R. Ruiz-García, J. Cano, J. Ferrando-Soria, E. Pardo, F. R. Fortea-Pérez, S.-E. Stiriba, M. Julve and F. Lloret, *Acc. Chem. Res.*, 2015, **48**, 510-520.
7. P. Gütlich, A. B. Gaspar and Y. Garcia, *Bail. J. Org. Chem.*, 2013, **9**, 342-391.
8. J. W. Sharples and D. Collison, *Coord. Chem. Rev.*, 2014, **260**, 1-20.
9. S. Kang, Y. Shiota, A. Kariyazaki, S. Kanegawa, K. Yoshizawa and O. Sato, *Chem. Eur. J.*, 2016, **22**, 532-538.
10. D. P. August, G. S. Nichol and P. J. Lusby, *Angew. Chem. Int. Ed.*, 2016, **55**, 15022-15026.

View Article Online
DOI: 10.1039/C7DT00293A

11. A. J. Metherell and M. D. Ward, *Dalton, Trans.*, 2016, **45**, 16096-16111.
12. P. Wei, X. Yan and F. Huang, *Chem. Soc. Rev.*, 2015, **44**, 815-832.
13. F. D'Souza and O. Ito, *Chem. Commun.*, 2009, 4913-4928.
14. C. J. Bruns and J. F. Stoddart, *Acc. Chem. Res.*, 2014, **47**, 2186-2199.
15. J. D. Crowley, S. M. Goldup, A.-L. Lee, D. A. Leigh and R. T. McBurney, *Chem. Soc. Rev.*, 2009, **38**, 1530-1541.
16. J. C. Lewis, *ACS Catalysis*, 2013, **3**, 2954-2975.
17. H. T. Chifotides and K. R. Dunbar, *Acc. Chem. Res.*, 2013, **46**, 894-906.
18. T. J. Mooibroek, C. A. Black, P. Gamez and J. Reedijk, *Cryst. Growth Des.*, 2008, **8**, 1082-1093.
19. P. Gamez, *Inorg. Chem. Front.*, 2014, **1**, 35-43.
20. A. Bauza, T. J. Mooibroek and A. Frontera, *CrystEngComm*, 2016, **18**, 10-23.
21. Y.-Z. Liu, K. Yuan, L.-L. Lv, Y.-C. Zhu and Z. Yuan, *The J. Phys. Chem. A*, 2015, **119**, 5842-5852.
22. T. Aoki, H. Sakai, K. Ohkubo, T. Sakanoue, T. Takenobu, S. Fukuzumi and T. Hasobe, *Chem. Sci.*, 2015, **6**, 1498-1509.
23. H. T. Chifotides, B. L. Schottel and K. R. Dunbar, *Angew. Chem. Int. Ed.*, 2010, **49**, 7202-7207.
24. G. Aragay, A. Frontera, V. Lloveras, J. Vidal-Gancedo and P. Ballester, *J. Am. Chem. Soc.*, 2013, **135**, 2620-2627.
25. B. Chiavarino, M. E. Crestoni, P. Maître and S. Fornarini, *Int. J. Mass Spectrom.*, 2013, **354–355**, 62-69.
26. Y. Zhao, C. Beuchat, Y. Domoto, J. Gajewy, A. Wilson, J. Mareda, N. Sakai and S. Matile, *J. Am. Chem. Soc.*, 2014, **136**, 2101-2111.
27. J. Mareda and S. Matile, *Chem. Eur. J.*, 2009, **15**, 28-37.
28. A. Mitra, C. T. Hubley, D. K. Panda, R. J. Clark and S. Saha, *Chem. Commun.*, 2013, **49**, 6629-6631.
29. J. Míšek, A. Vargas Jentzsch, S.-i. Sakurai, D. Emery, J. Mareda and S. Matile, *Angew. Chem. Int. Ed.*, 2010, **49**, 7680-7683.
30. S. Guha, F. S. Goodson, L. J. Corson and S. Saha, *J. Am. Chem. Soc.*, 2012, **134**, 13679-13691.
31. H. T. Chifotides, I. D. Giles and K. R. Dunbar, *J. Am. Chem. Soc.*, 2013, **135**, 3039-3055.
32. Y. Zhao, Y. Li, Z. Qin, R. Jiang, H. Liu and Y. Li, *Dalton, Trans.*, 2012, **41**, 13338-13342.
33. J. Zhao, J. Li, G. Li, J. Gao, S. L. A. Kjelleberg, S. C. J. Loo and Q. Zhang, *J. Heterocyclic Chem.*, 2015, **52**, 1699-1704.
34. R. Podgajny, D. Pinkowicz, B. Czarnecki, M. Kozieł, S. Chorąży, M. Wis, W. Nitek, M. Rams and B. Sieklucka, *Cryst. Growth Des.*, 2014, **14**, 4030-4040.
35. J. Zhao, G. Li, C. Wang, W. Chen, S. C. J. Loo and Q. Zhang, *RSC Adv.*, 2013, **3**, 9653-9657.
36. X. Lucas, A. Bauza, A. Frontera and D. Quinonero, *Chem. Sci.*, 2016, **7**, 1038-1050.
37. Y. Zhao, Y. Cotelle, A.-J. Avestro, N. Sakai and S. Matile, *J. Am. Chem. Soc.*, 2015, **137**, 11582-11585.
38. K. S. Lee, I. Lim, S. H. Han and T. W. Kim, *Org. Electron.*, 2014, **15**, 343-347.
39. M. E. Ali and P. M. Oppeneer, *The J. Phys. Chem. Lett.*, 2011, **2**, 939-943.
40. J. Martínez-Lillo, A. H. Pedersen, J. Faus, M. Julve and E. K. Brechin, *Cryst. Growth Des.*, 2015, **15**, 2598-2601.
41. C. Estarellas, A. Frontera, D. Quiñonero and P. M. Deyà, *Angew. Chem. Int. Ed.*, 2011, **50**, 415-418.
42. H. Tokoro and S.-i. Ohkoshi, *Dalton, Trans.*, 2011, **40**, 6825-6833.
43. S. Chorazy, J. J. Stanek, W. Nogaś, A. M. Majcher, M. Rams, M. Kozieł, E. Juszyńska-Gałązka, K. Nakabayashi, S.-i. Ohkoshi, B. Sieklucka and R. Podgajny, *J. Am. Chem. Soc.*, 2016, **138**, 1635-1646.
44. S. Chorazy, J. Wang and S.-i. Ohkoshi, *Chem. Commun.*, 2016, **52**, 10795-10798.
45. V. Martínez, I. Boldog, A. B. Gaspar, V. Ksenofontov, A. Bhattacharjee, P. Gütlich and J. A. Real, *Chem. Mater.*, 2010, **22**, 4271-4281.
46. J. E. Clements, J. R. Price, S. M. Neville and C. J. Kepert, *Angew. Chem. Int. Ed.*, 2014, **53**, 10164-10168.
47. G. Maurin-Pasturel, J. Long, Y. Guari, F. Godiard, M.-G. Willinger, C. Guerin and J. Larionova, *Angew. Chem. Int. Ed.*, 2014, **53**, 3872-3876.
48. B. Nowicka, M. Reczynski, M. Rams, W. Nitek, J. Zukrowski, C. Kapusta and B. Sieklucka, *Chem. Commun.*, 2015, **51**, 11485-11488.
49. S.-i. Ohkoshi, S. Takano, K. Imoto, M. Yoshikiyo, A. Namai and H. Tokoro, *Nat Photon*, 2014, **8**, 65-71.
50. Y. Yoshida, K. Inoue, K. Kikuchi and M. Kurmoo, *Chem. Mater.*, 2016, **28**, 7029-7038.
51. M. Savastano, P. Arranz-Mascaros, C. Bazzicalupi, A. Bianchi, C. Giorgi, M. L. Godino-Salido, M. D. Gutierrez-Valero and R. Lopez-Garzon, *RSC Adv.*, 2014, **4**, 58505-58513.
52. P. Arranz-Mascarós, C. Bazzicalupi, A. Bianchi, C. Giorgi, M.-L. Godino-Salido, M.-D. Gutiérrez-Valero, R. Lopez-Garzón and M. Savastano, *J. Am. Chem. Soc.*, 2013, **135**, 102-105.
53. J. L. Segura, R. Juarez, M. Ramos and C. Seoane, *Chem. Soc. Rev.*, 2015, **44**, 6850-6885.
54. P. S. Szalay, J. R. Galán-Mascarós, B. L. Schottel, J. Bacsa, L. M. Pérez, A. S. Ichimura, A. Chouai and K. R. Dunbar, *J. Cluster Sci.*, 2004, **15**, 503-530.
55. T. Okubo, S. Kitagawa, M. Kondo, H. Matsuzaka and T. Ishii, *Angew. Chem. Int. Ed.*, 1999, **38**, 931-933.
56. S. Furukawa, T. Okubo, S. Masaoka, D. Tanaka, H.-C. Chang and S. Kitagawa, *Angew. Chem. Int. Ed.*, 2005, **44**, 2700-2704.
57. P. S. Szalay, J. R. Galán-Mascarós, R. Clérac and K. R. Dunbar, *Synth. Met.*, 2001, **122**, 535-542.
58. J. R. Gallegos, A. H. Francis, N. W. Ockwig, P. G. Rasmussen, R. G. Raptis, P. R. Challen and I. Ouedraogo, *Synth. Met.*, 2009, **159**, 1667-1671.
59. A. B. P. Lever, *Inorganic electronic spectroscopy*, Elsevier, 1984.
60. B. Sieklucka, *J. Chem. Soc., Dalton Trans.*, 1997, 869-872.
61. R. Podgajny, B. Sieklucka and W. Lasocha, *J. Chem. Soc, Dalton Trans.*, 2000, 1799-1803.
62. A. V. Krukau, O. A. Vydrov, A. F. Izmaylov and G. E. Scuseria, *J. Chem. Phys.*, 2006, **125**, 224106.
63. K. Nakamaru, K. Jin, A. Tazawa and M. Kanno, *Bull. Chem. Soc. Jap.*, 1975, **48**, 3486-3490.
64. F. Ulatowski, K. Dąbrowa, T. Bałakier and J. Jurczak, *J. Org. Chem.*, 2016, **81**, 1746-1756.
65. S. Grimme, J. Antony, S. Ehrlich and H. Krieg, *J. Chem. Phys.*, 2010, **132**, 154104.
66. G. Kresse and J. Hafner, *Phys. Rev. B*, 1993, **47**, 558-561.
67. G. Kresse and J. Furthmüller, *Phys. Rev. B*, 1996, **54**, 11169-11186.
68. ADF2013, Theoretical Chemistry, Vrije Universiteit, Amsterdam, The Netherlands, http://www.scm.com.
69. C. Fonseca Guerra, J. G. Snijders, G. te Velde and E. J. Baerends, *Theor. Chem. Acc.*, 1998, **99**, 391-403.
70. G. te Velde, F. M. Bickelhaupt, E. J. Baerends, C. Fonseca Guerra, S. J. A. van Gisbergen, J. G. Snijders and T. Ziegler, *J. Comput. Chem.*, 2001, **22**, 931-967.

View Article Online
DOI: 10.1039/C7DT00293A

71. M. P. Mitoraj, A. Michalak and T. Ziegler, *J. Chem. Theory Comput.*, 2009, **5**, 962-975.
72. K. K. Jude T. Rademacher, Anthony W. Czarnik, *Synthesis*, 1994, **4**.
73. M. Llunell, D. Casanova, J. Cirera, J. Bofill, P. Alemany, S. Alvarez, M. Pinsky and D. Avnir, SHAPE v. 2.1. *Program for the Calculation of Continuous Shape Measures of Polygonal and Polyhedral Molecular Fragments*, University of Barcelona: Barcelona, Spain, 2013.
74. O. V. Dolomanov, L. J. Bourhis, R. J. Gildea, J. A. K. Howard and H. Puschmann, *J. Appl. Crystallogr.*, 2009, **42**, 339-341.

View Article Online
DOI: 10.1039/C7DT00293A

Graphical abstract

Anion-π recognition between $[M(CN)_6]^{3-}$ complexes and $HAT(CN)_6$: structural matching and electronic charge density modification

Jędrzej Kobylarczyk, Dawid Pinkowicz, Monika Srebro-Hooper, James Hooper, and Robert Podgajny*

The first example of an anion-π charge transfer (CT) system between an anionic complex and a multisite anion receptor in solid state and in solution was constructed basing on prediction of structural and electronic matching of the building blocks.